PCCP

PAPER

View Article Online
View Journal | View Issue

Cite this: *Phys. Chem. Chem. Phys.*, 2024, **26**, 5848

ZnO monolayer-supported single atom catalysts for efficient electrocatalytic hydrogen evolution reaction

Rongzhi Wang [a] and Jin-Cheng Zheng *[ab]

Received 29th October 2023,
Accepted 19th January 2024

DOI: 10.1039/d3cp05241a

rsc.li/pccp

Hydrogen is identified as one of the most promising sustainable and clean energy sources. The development of a hydrogen evolution reaction (HER) catalyst with high activity is essential to meet future needs. Considering the novel advantages of two-dimensional materials and the high catalytic activity of atomic transition metals, in this study, using density functional theory calculations, the HER on a single transition metal (10 different TM atoms) adsorbed and doped ZnO monolayer (ZnO-m) has been investigated. The Volmer–Tafel reaction mechanisms and strain engineering of the three best HER catalysts are also discussed. The results show that Pt@ZnO-m, Co-doped ZnO-m and Ir-doped ZnO-m with high stability all have a smaller absolute H adsorption free energy than Pt, and the optimal value of Pt@ZnO-m is −0.017 eV. The calculation of the reaction energy barriers shows that the Volmer–Tafel step is favorable. Co@ZnO-m and Ir@ZnO-m have high HER activity, the widest pH range, and acid–alkali resistance. Pt@ZnO-m and Co-doped ZnO-m maintain excellent HER performances in the strain range of −4% to 4%.

Introduction

With the expansion of industrial production, severe energy shortages and environmental pollution have become the focus of global attention in recent years, urgently requiring the establishment of a global clean and sustainable energy system.[1–4] From this perspective, hydrogen (H_2) energy, which has the highest gravimetric energy density among all chemical fuels, is regarded as an ultra-clean and powerful alternative to meet future fuel needs.[5–8] At present, the reaction of water splitting for hydrogen production is a mature, industrialized and cheap technology, and its efficiency mainly depends on the performance of the catalysts.[9,10] For the electrocatalytic hydrogen evolution reaction (HER), platinum (Pt)-based materials have emerged as effective electrocatalysts, but their practical application in large-scale production is limited by their high cost and low abundance.[11] Therefore, there is an urgent need to develop cheaper and more effective HER catalysts.[12,13]

Two-dimensional (2D) material-supported single atom catalysts (SACs) take full advantage of each atomic catalytic site, combine the unique geometrical and electronic properties of 2D materials, and have multiple characteristics of efficient catalysis.[14–18] For example, the high tunability of the coordination environment for catalytic activity engineering, the open structure for easy mass transfer, suitability for well-established advanced surface characterization, and high feasibility to reveal, illustrate, design, and implement particular catalytic mechanisms.[19–25] SACs supported by 2D materials are expected to provide higher selectivity and catalytic activity for the HER than traditional catalysts. Recently, a series of 2D substrates (graphene,[26,71] MoS_2,[27,72] C_3N,[73] MXene,[28] g-C_3N_4,[29] g-CN,[30] and h-BN[31]) anchored with various metal (Co,[26,71] Rh,[72] Ag,[73] Ni,[27] Pt,[28,29] Ti,[30] and Ru[31]) atoms have been proposed as HER catalysts with high efficiencies.

Among the emerging family of 2D materials, ZnO monolayers have attracted tremendous research interest due to their intrinsic advantages, such as non-toxicity, high stability,[32] and tunable electronic,[33] magnetic,[34] thermoelectric,[35] and optical properties by changing the thickness,[36] molecular adsorption,[34] and heteroatomic doping.[37] At ambient temperature and pressure, the most stable phase of bulk ZnO is wurtzite, which undergoes a phase transition to a non-polar graphene-like structure when the thickness is reduced to about 8 atomic layers.[38] ZnO monolayers have been fabricated on substrates (such as Ag(111),[38] Au(111),[39] Pd(111),[40] and graphene[41]) or suspended in graphene pores.[42] The monolayer ZnO is a semiconductor with a wide band gap, and when additional holes or electrons are introduced through heteroatom doping

[a] *Department of Physics, Fujian Provincial Key Laboratory of Theoretical and Computational Chemistry, Xiamen University, Xiamen 361005, China. E-mail: jczheng@xmu.edu.cn*
[b] *Department of Physics and Department of New Energy Science and Engineering, Xiamen University Malaysia, Sepang 43900, Malaysia*

or adsorption, the band gap can be greatly reduced.[43,44] ZnO in various phases and morphologies has long been used as a catalyst or catalyst support.[45] Combining the superior properties of 2D confinement and the stable, economical, and eco-friendly characteristics, the ZnO monolayer serves as a promising candidate substrate for SACs.

Due to the wide band gap of the ZnO monolayer, researchers have focused on its application in the photocatalytic HER and the transition metal-decorated ZnO monolayer SAC for the electrocatalytic HER, which has not been studied yet. In this work, we theoretically screened 10 candidates for efficient HER SACs built from different transition metal atoms embedded in ZnO monolayers. Specifically, we studied two intercalation methods, namely substitution of Zn atoms in the ZnO monolayer and adsorption on top of O atoms at the most stable site of the ZnO monolayer. It is worth noting that these transition metal atoms, containing 5 non-noble metals and 5 noble metals, are commonly used to build HER catalysts. Thereafter, we studied the stability of the SACs and their catalytic activity for the HER. Then, the effect of pH and strain on the HER activity was determined. The single Co and Ir atom adsorption systems (Co@ZnO-m, Ir@ZnO-m) exhibit high HER catalytic activity regardless of the acidic, neutral or alkaline environments. The single Fe and Ru atom substitution systems (Fe-doped ZnO-m, Ru-doped ZnO-m) showcase outstanding HER performance with the widest pH range under alkaline and acidic conditions, respectively. Moreover, Pt@ZnO-m, Co-doped ZnO-m and Ir-doped ZnO-m have higher structural stability and better HER activity than Pt, and the first two structures can still retain excellent catalytic ability under biaxial strain from −4% to 4%.

Computational methods

The first-principles calculations were performed based on density functional theory and implemented in the Vienna *Ab initio* Simulation package (VASP).[46] The projector-augmented wave (PAW) pseudopotential[47] was used and the generalized gradient approximation of the Perdew–Burke–Ernzerhof (PBE-GGA) method[48] was employed in the calculations. A 500 eV cut-off energy was set for the plane-wave basis set. The convergence accuracy for the energy and force was set to 10^{-4} eV and 0.01 eV Å^{-1}. A 5 × 5 × 1 Monkhorst–Pack *k*-mesh in the Brillouin zone was used for the optimization. The van der Waals interactions were described by an empirical correction in Grimme's scheme (DFT-D3).[49] To obtain the ideal electronic structure, the *U* values of the Zn 3d and O 2p orbitals were set to 11.6 and 7, respectively. At the same time, U = 3 eV was used to consider the Coulomb interaction effect on all doped transition metals.[50,51] There was a vacuum of 15 Å in both directions perpendicular to the periodic direction to avoid the interactions between adjacent cells.

The Gibbs free energy of hydrogen adsorption (ΔG_H) was calculated to evaluate HER performance. The free energy ΔG_H is defined as $\Delta G_H = \Delta E_H + \Delta E_{ZPE} - T\Delta S_H + \Delta G(pH)$, where ΔE_H, ΔE_{ZPE}, and ΔS_H are the hydrogen adsorption energy, the zero point energy (ZPE), and the entropy differences between the adsorbed state and the gas phase, respectively. The adsorption energy per H atom (ΔE_H) is defined as $\Delta E_H = E_{slab+H} - E_{slab} - 1/2E_{H_2}$, where E_{slab+H} and E_{slab} are the total energies of the SACs with and without the adsorbed H atoms, and E_{H_2} is the total energy of H_2 gas. ΔG(pH) is an additional barrier to the adsorption of one H atom and depends on the pH value of the electrolyte. $\Delta G_{pH} = pH \times k_B T \ln 10$, where k_B is the Boltzmann constant and T is the temperature (298.15 K). ΔG_{pH} equals 0 eV when pH = 0 and increases when the corresponding electrolyte is acidic, neutral or basic. The calculation method for ΔG_H used in the present work was validated in a previous study.[52] Thus, the formula can be rewritten as $\Delta G_H = \Delta E_H + 0.24 + \Delta G(pH)$. Furthermore, the exchange current density i_0 at pH = 0 is calculated as follows:[53]

$$i_0 = \frac{ek_0}{1 + \exp(|\Delta G_H|/k_B T)} \quad (1)$$

where the rate constant k_0 is set to 1.

To discuss the stability of TM-adsorbed and TM-doped ZnO monolayers, the adsorption energy (E_a) and substitution formation energy (E_F) were considered. E_a is the energy required to dissociate the TM adatom from the ZnO monolayer and move it away from the sheet. It was determined to assess the stability of the TM-adsorbed systems using eqn (2).

$$E_a = E_{ZnO\text{-}m(TM)} - E_{ZnO\text{-}m} - E_{TM} \quad (2)$$

where $E_{ZnO\text{-}m(TM)}$ and $E_{ZnO\text{-}m}$ refer to the total energies of the TM-adsorbed ZnO monolayer and ZnO monolayer, respectively, and E_{TM} is the energy of the isolated TM atom.

In our simulation, the formation energy of TM-substituted Zn is calculated by the following formula:

$$E_F = E(ZnO\text{-}m_{TM}) - E_{ZnO\text{-}m} + \mu_{Zn} - \mu_{TM} \quad (3)$$

where $E(ZnO\text{-}m_{TM})$ is the total energy of the TM-doped ZnO monolayer, $E_{ZnO\text{-}m}$ is the total energy of the ZnO monolayer, and μ_{Zn} and μ_{TM} are the chemical potentials of the isolated Zn and TM atom, respectively. Moreover, the chemical potentials of isolated Zn and TM atoms indicate their total energies. Specifically, we place an isolated Zn or TM atom into a 10 × 10 × 10 cell and calculate its energy.

The charge density difference (ρ_{diff}) on the SAC before and after the adsorption of H is calculated as follows:

$$\rho_{diff} = \rho(H@SAC) - \rho(SAC) - \rho(H) \quad (4)$$

where ρ(H@SAC), ρ(SAC) and ρ(H) are the charge densities of H@SAC, SAC and H, respectively.

Results and discussion

Structure and electronic properties of the ZnO monolayer

It is well-known that bulk ZnO adopts a wurtzite structure as its thermodynamically stable phase under ambient conditions. A primitive ZnO unit cell has been widely modeled using first-principles calculations, as shown in Fig. 1(a). The density of states (DOS) is computed to represent the electronic behavior of ZnO, and the calculated energy band gap is 3.374 eV, which

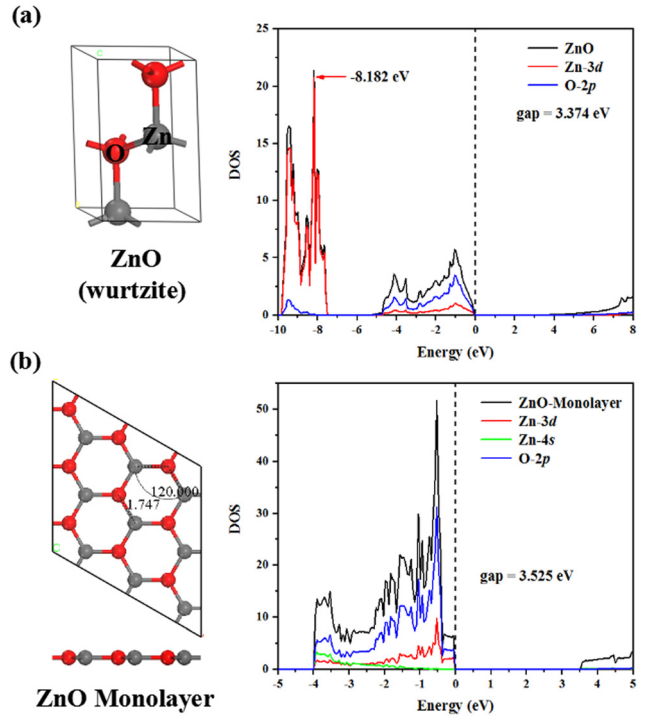

Fig. 1 (a) Crystal structure and electronic state of W–ZnO. (b) Atomic structure and electronic properties of the ZnO monolayer. The black dashed lines indicate the Fermi levels. The gray and red balls represent the Zn and O atoms, respectively.

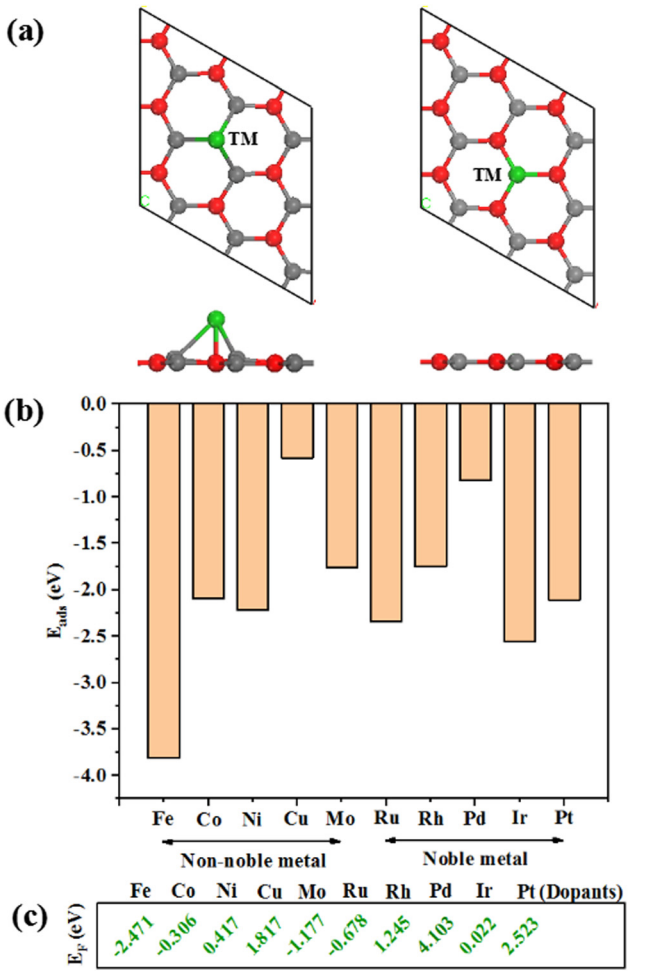

Fig. 2 (a) Top-view and side-view of the ZnO monolayer with a single transition metal atom adsorbed and doped. (b) Summarized adsorption energies of the ZnO monolayer-supported TM atoms. (c) The calculated formation energies of TM-substituted Zn atoms.

is in good agreement with the experimental value of 3.37 eV.[54] From a microscopic view, there are two main states that contribute to the valence band maximum, namely Zn-3d and O-2p. The highest peak of the Zn-3d states is −8.182 eV, which is very close to the experimental data of −8.2 eV.[55] Thereafter, we obtain the ZnO monolayer derived from bulk ZnO (Fig. 1(b)). The optimized ZnO monolayer has a planar honeycomb structure with the Zn–O bond length of 1.747 Å; meanwhile, similar to the DOS of the bulk ZnO, the upper valence bands are dominated by Zn-3d and O-2p states. The band gap of the ZnO monolayer was calculated to be 3.525 eV, which is close to the reported value of 3.576 eV[56] with GW corrections. Taken together, the above theoretical results indicate that the structure we adopted in our study is appropriate and accurate.

Stability of the single TM-adsorped and -doped ZnO monolayer

As shown in Fig. 2(a), ten different transition metal atoms (TM = Fe, Co, Ni, Cu, Mo, Ru, Rh, Pd, Ir and Pt) are used to adsorb on top of the O atom in the ZnO monolayer, which is tested as the most stable adsorption site. Besides, they are also used as substitutes for Zn atoms in ZnO monolayers to construct SAC models. Among the ten transition metal atoms, on the one hand, they are commonly used for constructing HER catalysts; on the other hand, they are divided into two parts: non-noble metals (Fe, Co, Ni, Cu, Mo) and noble metals (Ru, Rh, Pd, Ir, Pt). For structural analysis, TM adsorption could cause a small degree of structural distortion of the ZnO monolayer along with the formation of new TM–O and TM–Zn bonds. However, TM substitution may keep the ZnO monolayer planar with no distinct distortion. The diffusion and aggregation of the TM atoms in the SAC will reduce its catalytic activity and stability during catalytic reactions. To ensure that the single TM atom remains stable rather than diffusing or aggregating, we consider the adsorption energy (E_a) for TM adsorption and the substitution formation energy (E_F) for TM substitution. As depicted in Fig. 2(b), it is obvious that the adsorption energies of all TM adsorptions are negative, which indicates that the aggregation of TM atoms is hindered and the TM adsorption structures are thermodynamically stable. In addition, the Fe atom is most closely adsorbed to the ZnO monolayer and has the largest adsorption energy (E_a = −3.81 eV), while the Cu atom has the smallest adsorption energy (E_a = −0.577 eV). As for TM substitutions, the substitution formation energies are calculated, where the zero formation energy generally indicates that the dopants can be easily doped into the ZnO monolayer and can be stable in the system. As shown in Fig. 2(c), all metal atoms could be stably doped into the ZnO monolayer with relatively low

formation energies. Among them, the formation energy of the Ir-doped ZnO single-layer system is close to zero.

HER performances of the single TM-adsorbed and TM-doped ZnO monolayer

The HER activities of TM@ZnO-m and TM-doped ZnO-m are investigated as follows. It is well known that HER activity depends largely on the Gibbs free adsorption energy of an H atom.[57] Values close to zero correspond to better HER performance.[58] Currently, one of the most commonly used HER catalysts is Pt, whose theoretically calculated Gibbs free adsorption energy is about −0.09 eV.[59] One of the most important principles for designing new HER catalysts is that the absolute value of the Gibbs free adsorption energy is lower than or similar to that of Pt. Moreover, the HER catalytic activity is considered to be high if $|\Delta G_H| < 0.2$ eV.[60,61] In this study, H atoms were adsorbed on the top sites of the TM atoms. According to our calculation results, ΔG_H of TM@ZnO-m is shown in Fig. 3(a). The absolute ΔG_H values of Fe@ZnO-m, Mo@ZnO-m, Rh@ZnO-m and Pt@ZnO-m are less than 0.2 eV, and the corresponding values are 0.118, 0.198, −0.112 and −0.017 eV, respectively. On the one hand, these four structures exhibit good HER performance; on the other hand, Pt@ZnO-m has the lowest absolute ΔG_H, which is much smaller than that of Pt, indicating that Pt@ZnO-m can be a promising candidate for HER catalysts. However, Cu@ZnO-m and Pd@ZnO-m show very inert HER activities, as they possess the most negative and positive ΔG_H values among all TM@ZnO-m. The calculated ΔG_H values for TM-doped ZnO-m are shown in Fig. 3(b). It is obvious that, except for Co-doped ZnO-m, non-noble metal-doped ZnO-m is not suitable for the HER because the absolute ΔG_H is large. Surprisingly, Co-doped ZnO-m exhibits excellent HER performance with a ΔG_H of −0.031 eV. In comparison, noble metal-doped ZnO-m has relatively small absolute ΔG_H values of −0.202, 0.11, 0.444, −0.083 and 0.135 eV. Then, we found that Rh-doped ZnO-m, Ir-doped ZnO-m and Pt-doped ZnO-m exhibit high HER activity. In summary, Pt@ZnO-m, Co-doped ZnO-m and Ir-doped ZnO-m have extraordinary HER performance, even better than that of the state-of-the-art catalyst Pt.

In order to better understand the HER catalytic performance of the above structures, we use the volcano curves to describe the relationship between the exchange current density i_0 and ΔG_H. The model at the top of the volcano curve is considered to be the best configuration for the HER. As shown in Fig. 3(c), Pt@ZnO-m is at the top of the volcano curve with the largest exchange current density, which indicates its excellent HER performance. Cu@ZnO-m, Co@ZnO-m and Ir@ZnO-m display low exchange current densities due to large negative ΔG_H values. In other words, the intrinsic reason is that the H atom

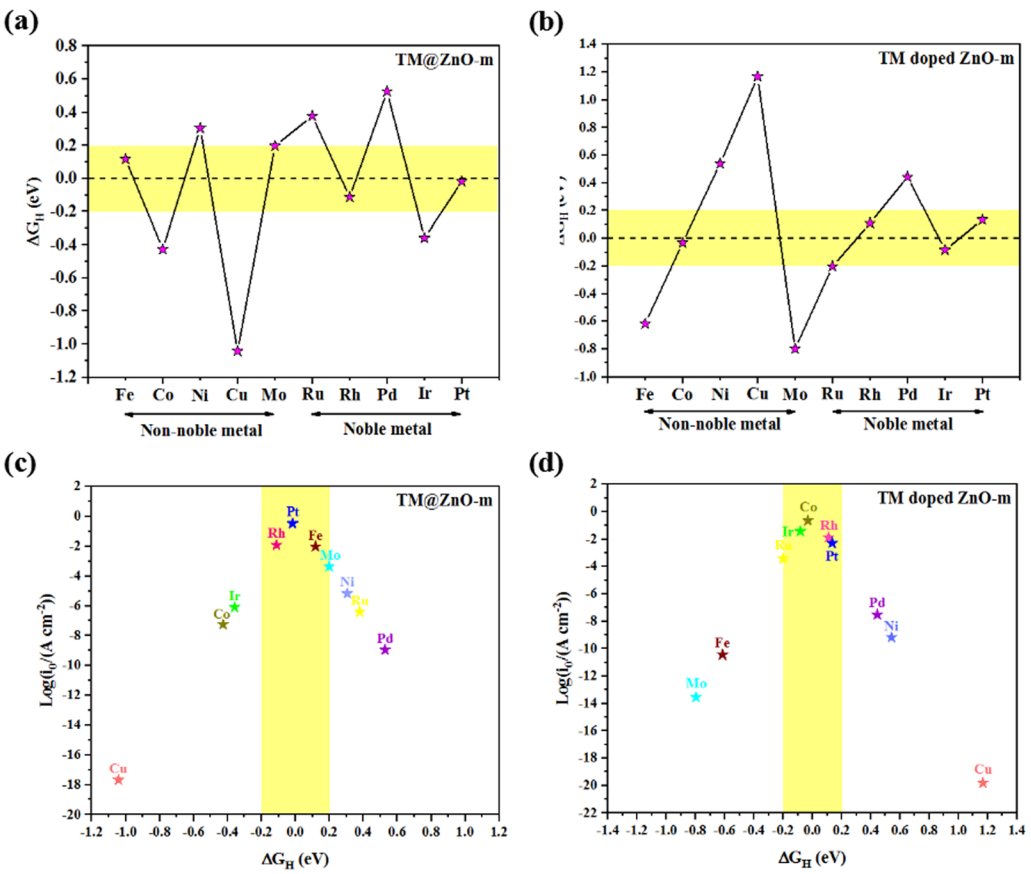

Fig. 3 Calculated Gibbs free energies (ΔG_H) of (a) TM@ZnO-m and (b) TM-doped ZnO-m for H adsorption. Volcano curves of the exchange current density i_0 of (c) TM@ZnO-m and (d) TM-doped ZnO-m as a function of ΔG_H.

is adsorbed too tightly in these three models. Meanwhile, Ni@ZnO-m, Ru@ZnO-m and Pd@ZnO-m also exhibit low current densities caused by large positive ΔG_H values. Here, the adsorption of H atoms on them is too weak. However, the situation of TM-doped ZnO-m is different from that of TM@ZnO-m when studying the exchange current density, as shown in Fig. 3(d). First, unlike Co@ZnO-m and Ir@ZnO-m, Co-doped ZnO-m and Ir-doped ZnO-m showcase high exchange current densities, which indicates their outstanding HER activity. Next, Fe-doped ZnO-m and Mo-doped ZnO-m show low current densities with large negative ΔG_H. Last but not least, Cu-doped ZnO-m, Ni-doped ZnO-m, Ru-doped ZnO-m and Pd-doped ZnO-m possess relative low current densities, which are consistent with the corresponding TM@ZnO-m systems. Overall, a good HER catalyst with a high exchange current density must possess moderate H adsorption energy, which is neither too strong nor too weak.

pH dependence of the HER

In electrocatalytic water splitting for H_2 production, the HER can be performed in acidic, basic or neutral media. Among these conditions, the HER in alkaline and neutral media is the most challenging because their kinetics are slowed down by the need for an additional water dissociation step. The most active HER catalyst in acidic media, platinum (Pt), shows two to three orders of magnitude lower activity when operated in neutral media.[62] Thus, studying the pH-dependent HER performance of the catalytic models is extremely important. To better understand the effect of pH on the HER performance of all modified ZnO-m samples, the pH-dependent ΔG_H was calculated. As shown in Fig. 4, the adsorption strengths of H atoms in different modified ZnO-m structures decrease with an increase of the pH value. The pH-dependent HER properties of TM@ZnO-m and TM-doped ZnO-m differed.

The relationship between ΔG_H and pH for non-noble metal@ZnO-m is shown in Fig. 4(a). In the pH range from 0 to 14, the lines of Ni@ZnO-m and Cu@ZnO-m are not located in the high HER activity range (−0.2 to 0.2 eV). For Co@ZnO-m, this line completely spans the high HER activity range and remains in acidic, basic and neutral media, indicating that Co@ZnO-m shows excellent HER activity with the widest pH range and acid–alkali resistance. The ΔG_H of Co@ZnO-m can be adjusted to zero when the pH is 7.237. The relationship between ΔG_H and pH for noble metal@ZnO-m is shown in Fig. 4(b). Compared with the model in Fig. 4(a) and (b) shows more suitable HER activity. Pt@ZnO-m, Rh@ZnO-m and Ir@ZnO-m exhibit excellent HER activities when the pH range is from 0 to 7, while Pd@ZnO-m and Ru@ZnO-m exhibit poor HER activities because their ΔG_H values are much larger than 0.2 eV in the whole pH range. Like Co@ZnO-m, Ir@ZnO-m also has excellent HER activity with the widest pH range and acid–alkali resistance. The ΔG_H of Ir@ZnO-m can be tuned to zero when the pH is 6.085. As shown in Fig. 4(c), compared to non-noble metal@ZnO-m,

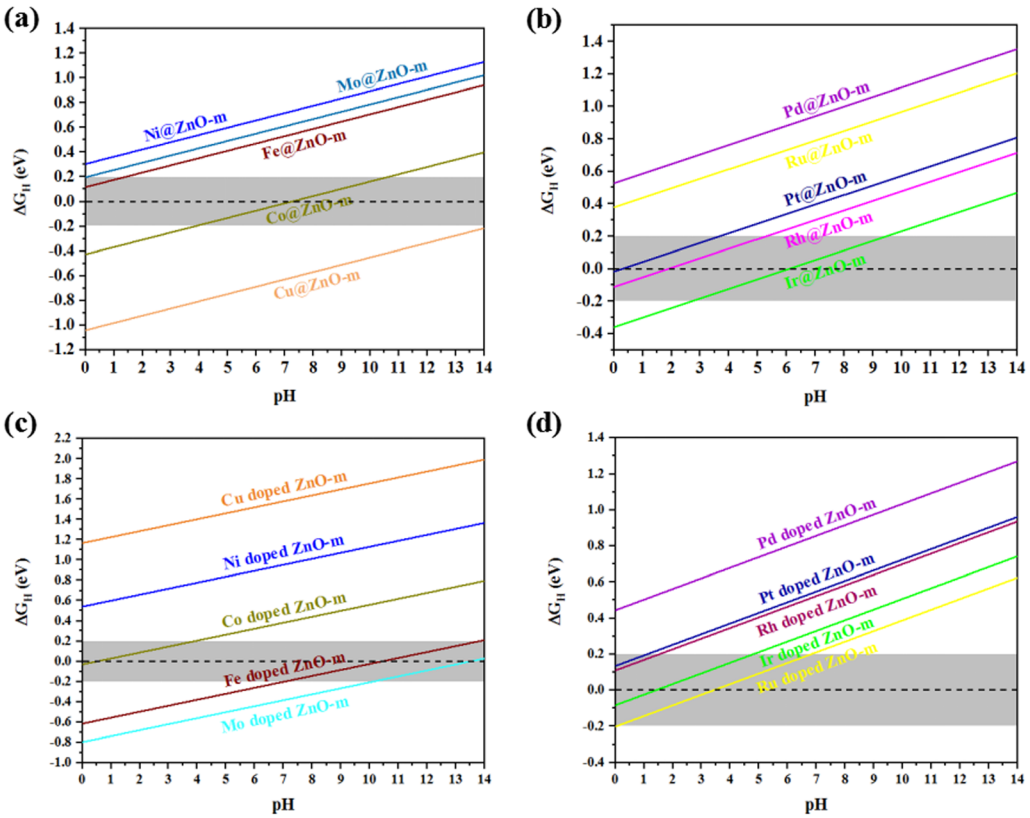

Fig. 4 The pH-dependent ΔG_H. (a) Non-noble metal@ZnO-m, (b) noble metal@ZnO-m, (c) non-noble metal-doped ZnO-m, and (d) noble metal-doped ZnO-m. The HER preferable area is shown in grey (−0.2 to 0.2 eV).

non-noble metal-doped ZnO-m show some similarities and differences. First, the lines of Ni-doped ZnO-m and Cu-doped ZnO-m are not located in the high HER activity range, which is the same as that of the corresponding non-noble metal adsorption structures. Then, Fe-doped ZnO-m and Mo-doped ZnO-m exhibit high HER activities when the pH ranges from 7 to 14, which indicates that they have highly alkaline HER performance. Besides, Fe-doped ZnO-m has the widest pH range among non-noble metal-doped ZnO-m. However, Fe@ZnO-m and Mo@ZnO-m show relatively good HER activities in acidic media. Moreover, unlike Co@ZnO-m, Co-doped ZnO-m has a much poorer alkaline HER activity. As shown in Fig. 4(d), apart from Pd-doped ZnO-m, it is obvious that Pt-doped ZnO-m, Rh-doped ZnO-m, Ir-doped ZnO-m and Ru-doped ZnO-m show high HER activity when the pH ranges from 0 to 7. Last but not least, Ru-doped ZnO-m shows excellent acidic HER activity over the widest pH range.

Electronic properties and HER mechanism analysis

In the SAC models we studied, Pt@ZnO-m, Co-doped ZnO-m and Ir-doped ZnO-m showed superior HER performance compared to Pt. Then, we focus on these three HER catalysts and analyze their electronic structures by calculating the density of states (DOS), including the total density of states (TDOS) and the partial density of states (PDOS). Additionally, we further explore their HER mechanisms. The charge density difference of H on Co-doped ZnO-m is also calculated to understand the electron distribution during the adsorption process. Judging from the TDOS depicted in Fig. 5(a)–(c), Pt@ZnO-m, Co-doped ZnO-m and Ir-doped ZnO-m all behave as metals without band gaps, and it is an amazing and fantastic phenomenon that these three modification ways could transition the ZnO-m semiconductor into a metal. Notably, Pt@ZnO-m, Co-doped ZnO-m and Ir-doped ZnO-m exhibit metallic properties attributed to the appearance of sharp DOS peaks at the Fermi level. The metallic conductivity enhances the efficiency of charge transportation for the HER, which accounts for their outstanding HER performance. Next, we mainly analyze the DOS peaks at the Fermi level by calculating the PDOS, as shown in Fig. 5(d)–(f). Pt-5d, Co-3d and Ir-5d orbitals are the main contributors to the DOS peaks. Therefore, the transition

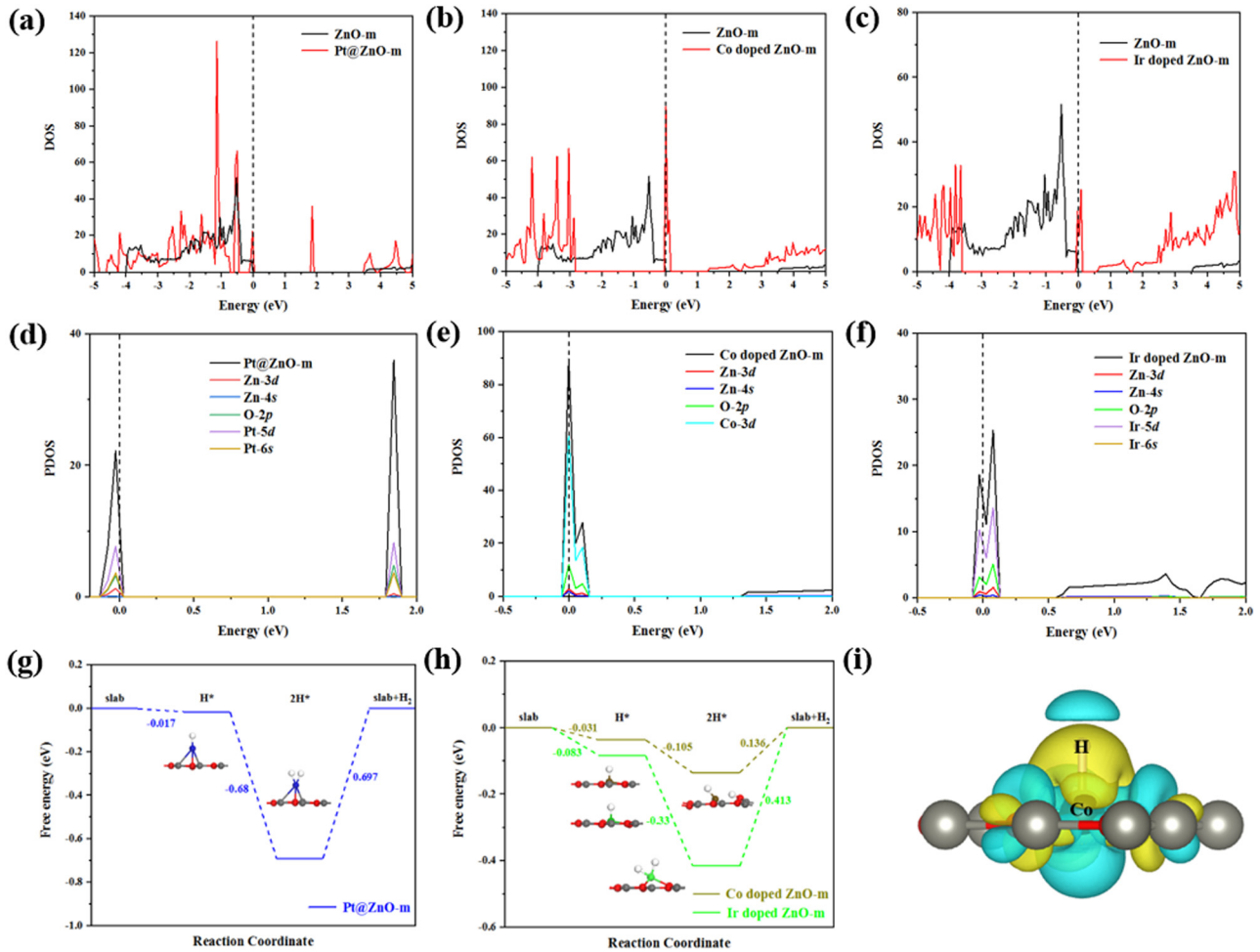

Fig. 5 The total density of states (TDOS) of (a) Pt@ZnO-m, (b) Co-doped ZnO-m, and (c) Ir-doped ZnO-m. The partial density of states (PDOS) of (d) Pt@ZnO-m, (e) Co-doped ZnO-m, and (f) Ir-doped ZnO-m. Vertical dashed lines represent the Fermi levels. The HER mechanism of (g) Pt@ZnO-m, and (h) Co-doped ZnO-m and Ir-doped ZnO-m. (i) Charge density difference of Co-doped ZnO-m after H atom adsorption (the isosurface is 0.001 e Å^{-3}) (the yellow region shows charge accumulation, and the blue region shows charge depletion).

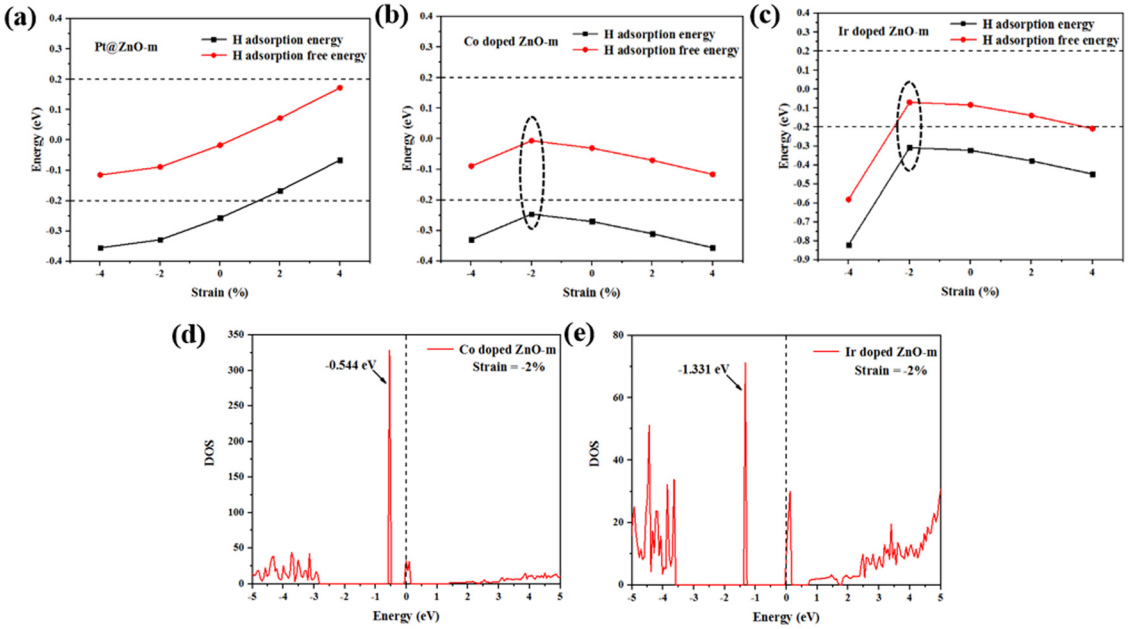

Fig. 6 Variation of the H adsorption energies and free energies as a function of (a) Pt@ZnO-m, (b) Co-doped ZnO-m, and (c) Ir-doped ZnO-m with strain. The DOS of (d) Co-doped ZnO-m with −2% strain and (e) Ir-doped ZnO-m with −2% strain. Vertical dashed lines represent the Fermi levels.

from the semiconductor to the conductor originates from the spare electrons in the d band of the introduced Pt, Co and Ir atoms. In addition, due to the overlap of the PDOS profiles of various atoms, there exist obvious hybridizations in the PDOS, such as Pt-5d and O-2p orbitals, Pt-5d and Zn-3d orbitals, Co-3d and O-2p orbitals, and Ir-5d and O-2p orbitals, representing Pt–O, Pt–Zn, Co–O, and Ir–O interactions.

In addition, we explore the HER mechanisms of these three models, as shown in Fig. 5(g) and (h). Due to the lower free energy, the adsorption of the second H atom on the surfaces of Pt@ZnO-m, Co-doped ZnO-m and Ir-doped ZnO-m is relatively simple, which indicates that the HER process may follow the Volmer–Tafel mechanism. In the first Volmer step, one H atom is adsorbed on the TM site. Then, the second H atom is also adsorbed on the TM sites, except for the TM-adjacent sites (O sites) for Co-doped ZnO-m. By adsorbing one H atom to adsorbing two H atoms, the energies of Pt@ZnO-m, Co-doped ZnO-m and Ir-doped ZnO-m gradually decrease, and the corresponding values are −0.68, −0.105 and −0.33 eV, respectively. The rate-determining step of the Volmer–Tafel mechanism is H_2 desorption and the calculated energy barriers are 0.697, 0.136 and 0.413 eV, respectively. All of these energy barriers are relatively low, comparable to that of Pt(111) (∼0.82 eV);[63] hence, H_2 desorption can easily occur on Pt@ZnO-m, Co-doped ZnO-m and Ir-doped ZnO-m.

Finally, the charge density difference of H on Co-doped ZnO-m is calculated to understand the electron distribution during the adsorption process. As can be seen from Fig. 5(i), an obvious charge accumulation region appears between the Co and H atoms and charge depletion is above the H atom and below the Co. Based on the above analysis, there is a certain degree of chemical interaction between Co and H with overlapping states and charge density redistribution, resulting in a zero approached ΔG_H, which is better than that of Pt.

The effect of strain on the HER activity

Strain engineering is a useful approach for tuning various properties of functional materials.[64–69] Recently, strain engineering has been shown to play a considerable role in optimizing HER performance.[70] Here, biaxial strains ranging from −4% to 4% are employed to explore the HER activity of Pt@ZnO-m, Co-doped ZnO-m and Ir-doped ZnO-m. The results are shown in Fig. 6(a)–(c). For Pt@ZnO-m, the H adsorption energy decreases gradually with increasing strain while ΔG_H shows the opposite trend. When the strain ranges from −4% to 4%, ΔG_H ranges from −0.116 to 0.173 eV, which is located in the high HER activity range (−0.2 to 0.2 eV). However, for Co-doped ZnO-m and Ir-doped ZnO-m, the H adsorption energy first decreased and then increased within the stress range. On the contrary, ΔG_H first increased and then decreased. Furthermore, Co-doped ZnO-m maintained high HER performance over the strain range, but Ir-doped ZnO-m did not. The inflection points are marked by black dotted coils, as shown in Fig. 6, and the corresponding strain is −2%. The possible intrinsic reasons are analyzed using DOS, as shown in Fig. 6(d) and (e). Compared to the DOSs of Co-doped ZnO-m and Ir-doped ZnO-m, it is clear that new and sharp DOS peaks appear at −0.544 and −1.331 eV below the Fermi level at −2% strain. Therefore, changes in the electronic structure may affect the catalytic activity of the material.

Conclusions

In conclusion, the potential use of TM-atomically adsorbed and TM-doped ZnO monolayers as electrocatalysts for the HER has

been systematically investigated using DFT calculations. All TM-adsorbed and -doped ZnO monolayers are energetically stable. The calculation of ΔG_H shows that the absolute ΔG_H values of Pt@ZnO-m, Co-doped ZnO-m and Ir-doped ZnO-m are all smaller than that of Pt, and the optimal value of Pt@ZnO-m is −0.017 eV. The exchange current density is highly correlated to ΔG_H and shows a volcano-like trend. The HER catalysts TM@ZnO-m, Co@ZnO-m and Ir@ZnO-m exhibit high HER activities with the widest pH range and acid–alkali resistance. The TM-doped ZnO-m, Fe-doped ZnO-m and Ru-doped ZnO-m show good HER performances with the widest pH range in alkaline and acidic media, respectively. Moreover, the Volmer–Tafel mechanism is favorable for Pt@ZnO-m, Co-doped ZnO-m and Ir-doped ZnO-m. Pt@ZnO-m and Co doped ZnO-m maintained excellent HER performances in the strain range of −4% to 4%. Through electronic structure analysis, the excellent HER activities of Pt@ZnO-m, Co-doped ZnO-m and Ir-doped ZnO-m are mainly attributed to their metallic properties. However, the transition from semiconductor to conductor originates from the spare electrons in the d band of the introduced Pt, Co and Ir atoms. Overall, our study suggests that single transition metal atom-adsorbed and -doped ZnO monolayers, especially Pt@ZnO-m, Co-doped ZnO-m and Ir-doped ZnO-m, have better HER activities than the existing noble metal catalysts, which can be advantageous for designing SACs with high catalytic performance.

Conflicts of interest

There are no conflicts of interest to declare.

Acknowledgements

This research is supported by the National Key R&D Program of China (grant no. 2022YFB3605403) and the National Natural Science Foundation of China (NSFC) (no. 12274355).

References

1 J. A. Turner, Sustainable Hydrogen Production, *Science*, 2004, **305**, 972–974.
2 S. Chu and A. Majumdar, Opportunities and challenges for a sustainable energy future, *Nature*, 2012, **488**, 294–303.
3 N. S. Lewis and D. G. Nocera, Powering the planet: chemical challenges in solar energy utilization, *Proc. Natl. Acad. Sci. U. S. A.*, 2006, **103**, 15729–15735.
4 T. R. Cook, D. K. Dogutan, S. Y. Reece, Y. Surendranath, T. S. Teets and D. G. Nocera, Solar Energy Supply and Storage for the Legacy and Nonlegacy Worlds, *Chem. Rev.*, 2010, **110**, 6474–6502.
5 N. Mahmood, Y. Yao, J.-W. Zhang, L. Pan, X. Zhang and J.-J. Zou, Electrocatalysts for Hydrogen Evolution in Alkaline Electrolytes: Mechanisms, Challenges, and Prospective Solutions, *Adv. Sci.*, 2017, **5**, 1700464.
6 Y. Lei, Y. Wang, Y. Liu, C. Song, Q. Li, D. Wang and Y. Li, Designing Atomic Active Centers for Hydrogen Evolution Electrocatalysts, *Angew. Chem., Int. Ed.*, 2020, **59**, 20794–20812.
7 Y. Shi, Z. R. Ma, Y. Y. Xiao, Y. C. Yin, W. M. Huang, Z. C. Huang, Y. Z. Zheng, F. Y. Mu, R. Huang, G. Y. Shi, Y. Y. Sun, X. H. Xia and W. Chen, Electronic metal-support interaction modulates single-atom platinum catalysis for hydrogen evolution reaction, *Nat. Commun.*, 2021, **12**, 3021.
8 S. Anantharaj and V. Aravindan, Developments and Perspectives in 3d Transition-Metal-Based Electrocatalysts for Neutral and Near-Neutral Water Electrolysis, *Adv. Energy Mater.*, 2020, **10**, 1902666.
9 M. S. Dresselhaus and I. L. Thomas, Alternative energy technologies, *Nature*, 2001, **414**, 332–337.
10 Q. Hu, K. Gao, X. Wang, H. Zheng, J. Cao, L. Mi, Q. Huo, H. Yang, J. Liu and C. He, Subnanometric Ru clusters with upshifted D band center improve performance for alkaline hydrogen evolution reaction, *Nat. Commun.*, 2022, **13**, 3958.
11 D. Voiry, H. S. Shin, K. P. Loh and M. Chhowalla, Low-dimensional catalysts for hydrogen evolution and CO_2 reduction, *Nat. Rev. Chem.*, 2018, **2**, 0105.
12 S. Wang, B. Xu, W. Huo, H. Feng, X. Zhou, F. Fang, Z. Xie, J. K. Shang and J. Jiang, Efficient FeCoNiCuPd thin-film electrocatalyst for alkaline oxygen and hydrogen evolution reactions, *Appl. Catal., B*, 2022, **313**, 121472.
13 L. Ju, M. Bie, X. Tang, J. Shang and L. Kou, Janus WSSe Monolayer: An Excellent Photocatalyst for Overall Water Splitting, *ACS Appl. Mater. Interfaces*, 2020, **12**, 29335–29343.
14 H. Xu, D. Cheng, D. Cao and X. C. Zeng, A universal principle for a rational design of single-atom electrocatalysts, *Nat. Catal.*, 2018, **1**, 339–348.
15 Q.-K. Li, X.-F. Li, G. Zhang and J. Jiang, Cooperative spin transition of monodispersed FeN_3 sites within graphene induced by CO adsorption, *J. Am. Chem. Soc.*, 2018, **140**, 15149–15152.
16 H. Liang, J. Wang, B. Jin, D. Li and Y. Men, Direct growth of Au nanoparticles on g-C_3N_4 for photocatalytic selective alcohol oxidations, *Inorg. Chem. Commun.*, 2019, **109**, 107574.
17 J. Wang, H. Liang, C. Zhang, B. Jin and Y. Men, Bi_2WO_{6-x} nanosheets with tunable Bi quantum dots and oxygen vacancies for photocatalytic selective oxidation of alcohols, *Appl. Catal., B*, 2019, **256**, 117874.
18 X. Cui, W. An, X. Liu, H. Wang, Y. Men and J. Wang, C_2N-graphene supported single-atom catalysts for CO_2 electrochemical reduction reaction: mechanistic insight and catalyst screening, *Nanoscale*, 2018, **10**, 15262–15272.
19 H. Li, Y. Shi, M.-H. Chiu and L.-J. Li, Emerging energy applications of two-dimensional layered transition metal dichalcogenides, *Nano Energy*, 2015, **18**, 293–305.
20 F. Wang, Z. Wang, Q. Wang, F. Wang, L. Yin, K. Xu, Y. Huang and J. He, Synthesis, properties and applications of 2D non-graphene materials, *Nanotechnology*, 2015, **26**, 292001.
21 B. Peng, P. K. Ang and K. P. Loh, Two-dimensional dichalcogenides for light-harvesting applications, *Nano Today*, 2015, **10**, 128–137.

22 C. Tan and H. Zhang, Two-dimensional transition metal dichalcogenide nanosheet-based composites, *Chem. Soc. Rev.*, 2015, **44**, 2713–2731.
23 R. Lv, H. Terrones, A. L. Elías, N. Perea-López, H. R. Gutiérrez, E. Cruz-Silva, L. P. Rajukumar, M. S. Dresselhaus and M. Terrones, Two-dimensional transition metal dichalcogenides: Clusters, ribbons, sheets and more, *Nano Today*, 2015, **10**, 559–592.
24 H. Liu, L. Wei, F. Liu, Z. Pei, J. Shi, Z.-J. Wang, D. He and Y. Chen, Homogeneous, heterogeneous, and biological catalysts for electrochemical N_2 reduction toward NH_3 under ambient conditions, *ACS Catal.*, 2019, **9**, 5245–5267.
25 A. Wang, J. Li and T. Zhang, Heterogeneous single-atom catalysis, *Nat. Rev. Chem.*, 2018, **2**, 65–81.
26 M. D. Hossain, Z. Liu, M. Zhuang, X. Yan, G.-L. Xu, C. A. Gadre, A. Tyagi, I. H. Abidi, C.-J. Sun, H. Wong, A. Guda, Y. Hao, X. Pan, K. Amine and Z. Luo, Rational Design of Graphene-Supported Single Atom Catalysts for Hydrogen Evolution Reaction, *Adv. Energy Mater.*, 2019, **9**, 1803689.
27 Q. Wang, Z. Zhao, S. Dong, D. He, M. J. Lawrence, S. Han, C. Cai, S. Xiang, P. Rodriguez, B. Xiang, Z. Wang, Y. Liang and M. Gu, Design of active Nickel single-atom decorated MoS_2 as a pH-universal catalyst for hydrogen evolution reaction, *Nano Energy*, 2018, **53**, 458–467.
28 J. Zhang, Y. Zhao, X. Guo, C. Chen, C.-L. Dong, R.-S. Liu, C.-P. Han, Y. Li, Y. Gogotsi and G. Wang, Single platinum atoms immobilized on an MXene as an efficient catalyst for the hydrogen evolution reaction, *Nat. Catal.*, 2018, **1**, 985–992.
29 X. Li, W. Bi, L. Zhang, S. Tao, W. Chu, Q. Zhang, Y. Luo, C. Wu and Y. Xie, Single-Atom Pt as Co-Catalyst for Enhanced Photocatalytic H_2 Evolution, *Adv. Mater.*, 2016, **28**, 2427–2431.
30 L. Zhang, X. Guo, S. Zhang and S. Huang, Identification of single-atom-anchored g-CN as pH universal photo- and electro- catalysts for hydrogen evolution, *Appl. Mater. Today*, 2021, **25**, 101177.
31 D. N. Sredojevic, M. R. Belic and Z. Sljivancanin, Hydrogen Evolution Reaction over Single-Atom Catalysts Based on Metal Adatoms at Defected Graphene and h-BN, *J. Phys. Chem. C*, 2020, **124**, 16860–16867.
32 K. B. Tom, S. Lin, L. F. Wan, J. Wang, N. Ahlm, A. T. N'Diaye, K. Bustillo, J. Huang, Y. Liu, S. Lou, R. Chen, S. Yan, H. Wu, D. Jin, H. Yuan, D. Prendergast and J. Yao, Solution-based, template-assisted realization of large-scale graphitic ZnO, *ACS Nano*, 2018, **12**, 7554–7561.
33 J. Lee, D. C. Sorescu and X. Deng, Tunable lattice constant and band gap of single- and few-layer ZnO, *J. Phys. Chem. Lett.*, 2016, **7**, 1335–1340.
34 Y.-H. Zhang, M.-L. Zhang, Y.-C. Zhou, J.-H. Zhao, S.-M. Fang and F. Li, Tunable electronic and magnetic properties of graphene-like ZnO monolayer upon doping and CO adsorption: a first-principles study, *J. Mater. Chem. A*, 2014, **2**, 13129–13135.
35 Y. L. Li, Z. Fan and J. C. Zheng, Enhanced thermoelectric performance in graphitic ZnO(0001) nanofilms, *J. Appl. Phys.*, 2013, **113**, 083705.
36 Q. Yao, Y. Liu, R. Lu, C. Xiao, K. Deng and E. Kan, Will a graphitic-like ZnO single-layer be an ideal substrate for graphene?, *RSC Adv.*, 2014, **4**, 17478–17482.
37 H. Guo, Y. Zhao, N. Lu, E. Kan, X. C. Zeng, X. Wu and J. Yang, Tunable magnetism in a nonmetal-substituted ZnO monolayer: A first-principles study, *J. Phys. Chem. C*, 2012, **116**, 11336–11342.
38 C. Tusche, H. L. Meyerheim and J. Kirschner, Observation of depolarized ZnO(0001) monolayers: Formation of unreconstructed planar sheets, *Phys. Rev. Lett.*, 2007, **99**, 026102.
39 H. Wu, Q. Fu, Y. Li, Y. Cui, R. Wang, N. Su, L. Lin, A. Dong, Y. Ning, F. Yang and X. Bao, Controlled growth of uniform two-dimensional ZnO overlayers on Au(111) and surface hydroxylation, *Nano Res.*, 2019, **12**, 2348–2354.
40 G. Weirum, G. Barcaro, A. Fortunelli, F. Weber, R. Schennach, S. Surnev and F. P. Netzer, Growth and surface structure of zinc oxide layers on a Pd(111) surface, *J. Phys. Chem. C*, 2010, **114**, 15432–15439.
41 H.-K. Hong, J. Jo, D. Hwang, J. Lee, N. Y. Kim, S. Son, J. H. Kim, M.-J. Jin, Y. C. Jun, R. Erni, S. K. Kwak, J.-W. Yoo and Z. Lee, Atomic scale study on growth and heteroepitaxy of ZnO monolayer on graphene, *Nano Lett.*, 2017, **17**, 120–127.
42 H. T. Quang, A. Bachmatiuk, A. Dianat, F. Ortmann, J. Zhao, J. H. Warner, J. Eckert, G. Cunniberti and M. H. Rümmeli, In situ observations of free-standing graphene-like mono- and bilayer ZnO membranes, *ACS Nano*, 2015, **9**, 11408–11413.
43 L. Chen, X. Zhang, Z. Xiong, Y. Liu, Y. Cui and B. Liu, Noble metal dopants modified two-dimensional zinc oxide: Electronic structures and magnetic properties, *J. Alloys Compd.*, 2019, **798**, 149–157.
44 L. Chen, A. Wang, Z. Xiong, S. Shi and Y. Gao, Effect of hole doping and strain modulations on electronic structure and magnetic properties in ZnO monolayer, *Appl. Surf. Sci.*, 2019, **467–468**, 22–29.
45 Y. Zhao, N. Liu, S. Zhou and J. Zhao, Two-dimensional ZnO for the selective photoreduction of CO_2, *J. Mater. Chem. A*, 2019, **7**, 16294–16303.
46 G. Kresse and J. Hafner, *Ab initio* molecular dynamics for liquid metals, *Phys. Rev. B: Condens. Matter Mater. Phys.*, 1993, **47**, 558.
47 G. Kresse and D. Joubert, From ultrasoft pseudopotentials to the projector augmented-wave method, *Phys. Rev. B: Condens. Matter Mater. Phys.*, 1999, **59**, 1758.
48 J. P. Perdew, K. Burke and M. Ernzerhof, Generalized Gradient Approximation Made Simple, *Phys. Rev. Lett.*, 1996, **77**, 3865.
49 S. Grimme, S. Ehrlich and L. Goerigk, Effect of the damping function in dispersion corrected density functional theory, *J. Comput. Chem.*, 2011, **32**, 1456–1465.
50 J. Zhou and Q. Sun, Magnetism of phthalocyanine-based organometallic single porous sheet, *J. Am. Chem. Soc.*, 2011, **133**, 15113–15119.
51 X. Zhang, Z. Bao, X. Ye, W. Xu, Q. Wang and Y. Liu, Half-metallic properties of 3*d* transition metal atom-intercalated graphene@MS_2 (M = W, Mo) hybrid structures, *Nanoscale*, 2017, **9**, 11231–11238.

52 J. K. Nørskov, T. Bligaard, A. Logadottir, J. R. Kitchin, J. Chen, S. Pandelov and U. Stimming, Trends in the exchange current for hydrogen evolution, *J. Electrochem. Soc.*, 2005, **152**, J23–J26.
53 B. Zhang, X. Fu, L. Song and X. Wu, Improving hydrogen evolution reaction performance by combining ditungsten carbide and nitrogen-doped graphene: A first-principles study, *Carbon*, 2021, **172**, 122–131.
54 Ü. Özgür, Ya. I. Alivov, C. Liu, A. Teke, M. A. Reshchikov, S. Doğan, V. Avrutin, S.-J. Cho and H. Morkoç, A comprehensive review of ZnO materials and devices, *J. Appl. Phys.*, 2005, **98**, 041301.
55 M. Ruckh, D. Schmid and H. W. Schock, Photoemission studies of the ZnO/CdS interface, *J. Appl. Phys.*, 1994, **76**, 5945–5948.
56 Z. C. Tu, First-principles study on physical properties of a single ZnO monolayer with graphene-like structure, *J. Comput. Theor. Nanosci.*, 2010, **7**, 1182–1186.
57 J. Zhu, L. Hu, P. Zhao, L. Y. S. Lee and K. Wong, Recent advances in electrocatalytic hydrogen evolution using nanoparticles, *Chem. Rev.*, 2020, **120**, 851–918.
58 X. Zhang, A. Chen, Z. Zhang, M. Jiao and Z. Zhou, Transition metal anchored C_2N monolayers as efficient bifunctional electrocatalysts for hydrogen and oxygen evolution reactions, *J. Mater. Chem. A*, 2018, **6**, 11446–11452.
59 P. Wang, X. Zhang, J. Zhang, S. Wan, S. Guo, G. Lu, J. Yao and X. Huang, Precise tuning in platinum-nickel/nickel sulfide interface nanowires for synergistic hydrogen evolution catalysis, *Nat. Commun.*, 2017, **8**, 14580.
60 Q. Peng, J. Zhou, J. Chen, T. Zhang and Z. Sun, Cu single atoms on Ti_2CO_2 as a highly efficient oxygen reduction catalyst in a proton exchange membrane fuel cell, *J. Mater. Chem. A*, 2019, **7**, 26062–26070.
61 G. Gao, A. P. O'Mullane and A. Du, 2D MXenes: a new family of promising catalysts for the hydrogen evolution reaction, *ACS Catal.*, 2017, **7**, 494–500.
62 R. Subbaraman, D. Tripkovic, D. Strmcnik, K.-C. Chang, M. Uchimura, A. P. Paulikas, V. Stamenkovic and N. M. Markovic, Enhancing hydrogen evolution activity in water splitting by tailoring Li^+–$Ni(OH)_2$–Pt interfaces, *Science*, 2011, **334**, 1256–1260.
63 K. Chan and J. K. Nørskov, Electrochemical barriers made simple, *J. Phys. Chem. Lett.*, 2015, **6**, 2663–2668.
64 J. C. Zheng and Y. Zhu, Searching for a higher superconducting transition temperature in strained MgB_2, *Phys. Rev. B: Condens. Matter Mater. Phys.*, 2006, **73**, 024509.
65 N. Wei, L. Xu, H. Q. Wang and J. C. Zheng, Strain engineering of thermal conductivity in graphene sheets and nanoribbons: a demonstration of magic flexibility, *Nanotechnology*, 2011, **22**, 105705.
66 T. Y. Lü, X. X. Liao, H. Q. Wang and J. C. Zheng, Tuning the indirect-direct band gap transition of SiC, GeC and SnC monolayer in a graphene-like honeycomb structure by strain engineering: a quasiparticle GW study, *J. Mater. Chem.*, 2012, **22**, 10062–10068.
67 J. J. Li, Y. Dai and J. C. Zheng, Strain engineering of ion migration in $LiCoO_2$, *Front. Phys.*, 2022, **17**, 13503.
68 H. Cheng and J. C. Zheng, Ab initio study of anisotropic mechanical and electronic properties of strained carbon–nitride nanosheet with interlayer bonding, *Front. Phys.*, 2021, **16**, 43505.
69 W. Zhang, F. Y. Du, Y. Dai and J. C. Zheng, Strain engineering of Li ion migration in olivine phosphates cathode materials $LiMPO_4$ (M = Mn, Fe, Co) and $(LiFePO_4)_n(LiMnPO_4)_m$ superlattices, *Phys. Chem. Chem. Phys.*, 2023, **25**, 6142–6152.
70 D. Er, H. Ye, N. C. Frey, H. Kumar, J. Lou and V. B. Shenoy, Prediction of Enhanced Catalytic Activity for Hydrogen Evolution Reaction in Janus Transition Metal Dichalcogenides, *Nano Lett.*, 2018, **18**, 3943–3949.
71 D. H. Md, Z. Liu, M. Zhuang, X. Yan, G.-L. Xu, A. G. Chaitanya, T. Abhishek, H. A. Irfan, C.-J. Sun, H. Wong, G. Alexander, Y. Hao, X. Pan, A. Khalil and Z. Luo, Rational Design of Graphene-Supported Single Atom Catalysts for Hydrogen Evolution Reaction, *Adv. Energy Mater.*, 2019, **9**, 1803689.
72 Y. Wang, M. Wang, Z. Lu, D. Ma and Y. Jia, Enabling multifunctional electrocatalysts by modifying the basal plane of unifunctional 1T'-MoS_2 with anchored transition metal single atoms, *Nanoscale*, 2021, **13**, 13390–13400.
73 Y. Zhao, D. Ma, J. Zhang, Z. Lu and Y. Wang, Transition metal embedded C_3N monolayers as promising catalysts for the hydrogen evolution reaction, *Phys. Chem. Chem. Phys.*, 2019, **21**, 20432–20441.